measured. The soft sample is backed by foam so that it can be flat-mounted in a sample holder. The sample is placed such that the orientation of the fibres is vertical to the ground. The reconstructed data are given in Figure 9.

Because four transverse parameters (ε^r_{xx}, μ^r_{yy}) and (ε^r_{yy}, μ^r_{xx}) of this sample are unknown beforehand, the (ε^r_{xx}, μ^r_{yy}) and (ε^r_{yy}, μ^r_{xx}) obtained above are used to calculate the reflectivity of the sample backed by a metal flat plate versus frequency by using the formulas in [7], which are compared with the measured ones, as shown in Figure 10. It is seen that the difference for both of them is less than 0.6 dB on the whole. Thus the accuracy of the reconstructed parameters is checked and the effectiveness of this method is indirectly verified from the experiment.

4. CONCLUSION

A new free-space method for the measurement of biaxial material at microwave frequencies has been proposed in this paper. Four complex transverse constitutive parameters were directly computed from the measured reflection and transmission coefficients of a planar sample in free space for the normally incident plane wave with two polarizations. A free-space measurement system operating in the 8.2–12-GHz frequency range was set up and this method was experimentally verified.

If the PCS to characterize biaxial material does not coincide with the MCS, then the original biaxial material in PCS will become the nonbiaxial one in MCS; therefore, some approaches to determine the PCS need to be found to ensure the practicability of this method.

Since the reflection and transmission coefficients of thin planar biaxial material are hardly affected by the longitudinal parameters, the longitudinal parameters cannot be correctly reconstructed via free-space measurement of a thin planar sample. Future work will address how to realize the reconstruction of biaxial materials.

ACKNOWLEDGMENTS

The authors would like to acknowledge helpful discussions with Prof. G. T. Yin, Prof. Z. H. Xiao, and Prof. C. M. Dai of the National Electromagnetic Scattering Laboratory, Beijing, P. R. China.

REFERENCES

1. L. Cullen, A new free-space method for ferrite measurement of millimeter wavelength, Radio Sci 22 (1987), 1168–1170.
2. J.C. Joseph, R.J. Jost, and E.L. Utt, Multiple angle of incidence measurement technique for the permittivity and permeability of lossy materials at millimeter wavelengths, IEEE AP-S Int Symp Diag (1987), 640–643.
3. K. Ghodgaonkar, V.V. Varadan, and V.K. Varadan, A free-space method for measurement of dielectric constants and loss tangents at microwave frequencies, IEEE Trans Instrum Meas 37 (1989), 789–793.
4. K. Ghodgaonkar, V.V. Varadan, and V.K. Varadan, Free-space measurement of complex permittivity and complex permeability of magnetic materials at microwave frequencies, IEEE Trans Instrum Meas 39 (1990), 387–394.
5. P. Corona, F.D. Agostino, G. Ferrara, C. Gennarelli, and G. Riccio, Backscattering by dielectric-loaded trihedral corners and application to permittivity measurements, Microwave Opt Technol Lett 22 (1999), 361–367.
6. X.G. Liu, H.P. Guo, and H.C. Yin, A uniform presentation of reflection and transmission coefficients of planar anisotropic materials, Res Target Environmental Features (Chinese ed.) 1 (2003), 7–14.
7. H.C. Yin, P.K. Huang, X.G. Liu, and H.P. Guo, PO solution for scattering by complex object coated with anisotropic materials, J Syst Engig Electron 14 (2003), 1–7.

DUAL-BAND MILLIMETER-WAVE/INFRARED FOCAL-PLANE ARRAYS

M. Abdel-Rahman, B. Lail, and G. D. Boreman
Infrared Systems Lab/CREOL
University of Central Florida
Orlando, FL 32816

Received 18 December 2004

ABSTRACT: *In this paper, a novel arrangement for dual-band millimeter-wave and infrared focal plane array based on slot-antenna-coupled metal-oxide-metal diodes is demonstrated. The receiving properties for millimeter-wave and infrared antenna-coupled detector pixels are presented.* © 2005 Wiley Periodicals, Inc. Microwave Opt Technol Lett 46: 78–80, 2005; Published online in Wiley InterScience (www.interscience.wiley.com). DOI 10.1002/mop.20906

Key words: *dual-band antenna; focal plane array; MOM diode*

1. INTRODUCTION

The millimeter-wave (MMW) and infrared (IR) portions of the spectrum both have advantages for the development of imaging systems. Because of the difference in wavelengths, infrared imagers offer inherently high resolution, while millimeter-wave systems have better penetration through atmospheric aerosols such as fog and smoke. Shared-aperture imaging systems employing a common focal-plane array (FPA) that responds to both wavebands are desirable from the viewpoint of overall size and weight. Due to the growing interest in antenna-coupled detectors because of their speed and other capabilities related to their antenna properties, antenna-coupled detectors were recently implemented on FPAs for MMW [1] and IR [2] imaging applications.

In previous works [3, 4], we have developed slot-antenna-coupled metal-oxide-metal (MOM) diodes for simultaneous dual-band response at 28 THz and 94 GHz. The optimum spatial-sampling interval presents a challenge when implementing dual-band detectors on true FPA imagers. The spatial-sampling interval is on the order of tens of microns at 28 THz and a few millimeters at 94 GHz. The purpose of this work is to develop a focal plane-array arrangement that is capable of accommodating both MMW and IR antenna-coupled detectors. The FPA arrangement is

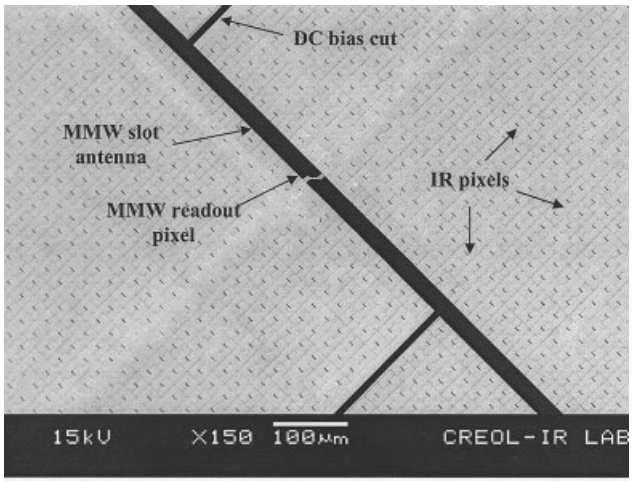

Figure 1 MMW slot antenna/IR slot antennas for a dual-band MMW/IR FPA

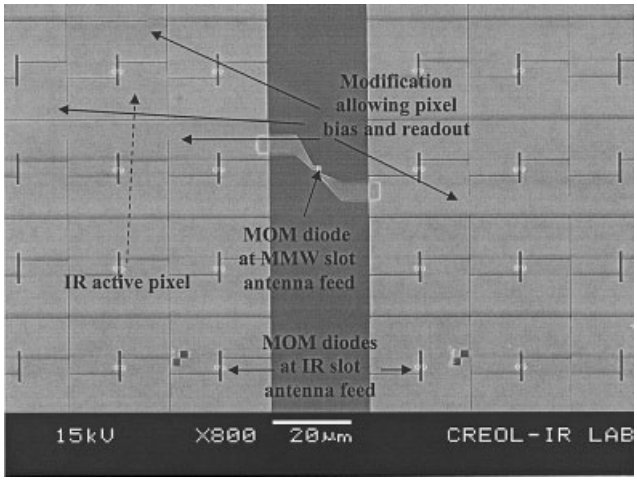

Figure 2 FPA configuration showing modification to allow for MMW and IR pixel readouts (the MMW sensor is located at the feed of the MMW slot antenna). A 4 × 4 array of IR pixels is populated with MOM diodes with one IR pixel made active

based on our slot-antenna-coupled MOM diodes developed previously [3, 4] for simultaneous response at 28 THz and 94 GHz. In this work, we demonstrate a focal plane with interleaved infrared and millimeter-wave sensors by fabricating infrared slot antennas in the ground plane of a millimeter-wave slot antenna.

2. DESIGN AND EXPERIMENTAL RESULTS

We designed and fabricated the FPA arrangement shown in Figure 1. The devices were fabricated on high-resistivity silicon substrates using electron-beam lithography. The fabrication process is detailed in [3, 4]. A MMW slot antenna/IR slot antennas configuration is used. One MMW pixel contains an MMW slot antenna in a 3 × 3 mm ground plane. The ground plane of the MMW slot antenna is slotted to contain 120 × 120 IR pixels, each with an area of 25 × 25 μm. Only 5% of the area utilized as a ground plane by the MMW slot antenna will be slotted for placing the IR detectors, and only 1.1% of the IR detectors will be removed in order to place the MMW slot. This arrangement is flexible for various IR pixel sizes. In the proposed design (Fig. 2), a MOM diode is placed at the feed of the MMW slot antenna. A 4 × 4 array of IR pixels is populated with MOM diodes where only one IR pixel is made active. The slotted separations between the IR pixels are 200-nm wide, which corresponds to $\lambda/15000$ at 94 GHz. In a true FPA, pixels are biased through via holes connected to the read-out integrated-circuit (ROIC). In our arrangement, we have modified some rows and columns of the pixels adjacent to the active MMW and IR pixels. These modifications allow us to bias the sensors on the active pixels.

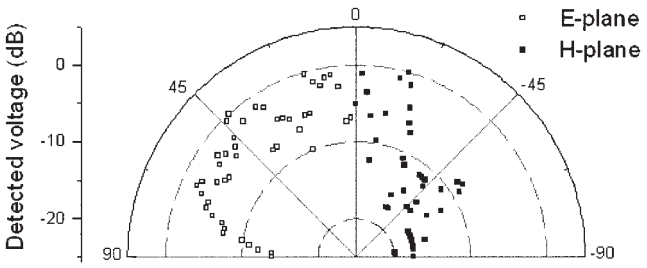

Figure 3 E- and H-plane patterns for the FPA MMW slot antenna

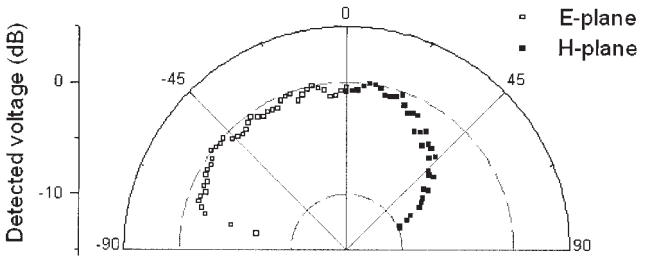

Figure 4 E- and H-plane patterns for the FPA IR slot antenna

The response of the MMW slot-antenna-coupled MOM diode embedded in the FPA structure was measured and compared to a regular MMW slot-antenna-coupled MOM diode. Both antennas had similar dimensions. The response of the regular MMW slot-antenna-coupled MOM was found to be three times higher than the response of the FPA MMW slot-antenna-coupled MOM. The slotted ground plane for the MMW slot antenna was modeled [5] as a homogenous ground-plane material. The conductivity of the material was altered and, meanwhile, the antenna efficiency was monitored. The antenna efficiency was found to decrease by a factor of three when the conductivity of the ground-plane material is decreased from $5 \times 10^7\ \Omega^{-1} \cdot m^{-1}$ to $3 \times 10^5\ \Omega^{-1} \cdot m^{-1}$. The decrease in antenna efficiency can correspond to the decrease in the responsivity of the detector.

The polarization sensitivity was further examined. The MMW slot antenna has a polarization ratio of 6:1 and the IR slot antenna shows weak polarization sensitivity with a polarization ratio of 1.4:1. The weak polarization ratio in the IR pixels can be attributed to the horizontal DC bias cuts that are comparable in length with the vertically placed IR slot antenna. The reception patterns were also measured. The E- and H-plane patterns for an FPA MMW slot are measured and plotted in Figure 3. The patterns have a multilobe radiation behavior, which may result from the power lost by the MMW slot antenna to surface waves. The IR slot-antenna E- and H-plane patterns are also measured and plotted, as shown in Figure 4. The E-plane pattern was found to be broader than the H-plane pattern. The simultaneous response was verified by modulating the MMW and IR radiation at two different frequencies and having them simultaneously incident on the FPA. The spectrum-analyzer output of the detected voltage indicated dual-band response.

3. SUMMARY

An antenna-coupled dual-band MMW and IR detector FPA arrangement has been designed, fabricated, and tested, demonstrating simultaneous dual-band response. The electromagnetic modeling has shown a change in the efficiency of MMW antenna due to the slotted nature of the MMW antenna ground plane.

ACKNOWLEDGMENT

This work was sponsored by DARPA/ARO under contract no. DAAD19-02-1-0232.

REFERENCES

1. F.J. González, Antenna-coupled infrared focal plane array, Ph.D. dissertation, University of Central Florida, 2003.
2. E.N. Grossman, A. Luukanen, and A.J. Miller, Active millimeter-wave video rate imaging with a staring 120 element microbolometer array, SPIE Proc 5410 (2004).

3. M.R. Abdel-Rahman, F.J. González, and G.D. Boreman, Antenna-coupled metal-oxide-metal for dual-band detection at 92.5 GHz and 28 THz, IEE Electron Lett 40 (2004), 116–118.
4. M. Abdel-Rahman, F.J. González, G. Zummo, C. Middleton, and G.D. Boreman, Antenna-coupled MOM diodes for dual-band detection in MMW and LWIR, SPIE Proc 5410 (2004).
5. Zeland Software Inc., IE3D simulator, 2004.

A 5-GHz INJECTION-LOCKED PHASE-LOCKED LOOP

Fotis Plessas and Grigorios Kalivas
Department of Electrical and Computer Engineering
University of Patras
Rion 26500, Greece

Received 21 December 2004

ABSTRACT: *In this paper, we introduce a 5-GHz injection-locked phase-locked loop (ILPLL). A new method is presented for accurate analysis of the phase-noise performance of the proposed system. Furthermore, comparison with other phase-noise-estimation techniques demonstrates that our method provides an accurate characterization of any ILPLL topology. The theoretical and calculation results show an improved performance for phase noise, locking range, and power consumption compared to conventional phase-locked loops (PLLs) and injection-locked oscillators (ILOs). Furthermore, we demonstrate the pulling behavior of the injected oscillator and examine the obtained results. To verify the presented analysis, a 5-GHz prototype has been implemented, which achieves −119-dBc/Hz at 100-KHz frequency offset, producing +4.5 dBm of output power and consuming 9 mA at 3 V.* © 2005 Wiley Periodicals, Inc. Microwave Opt Technol Lett 46: 80–84, 2005; Published online in Wiley InterScience (www.interscience.wiley.com). DOI 10.1002/mop.20907

Key words: *frequency synthesizer; injection-locked oscillator; injection-locked phase-locked loop; locking range; phase noise; transfer function; voltage-controlled oscillator*

1. INTRODUCTION

A promising technique for realizing low-phase-noise levels and increased locking range is the injection-locked phase-locked loop (ILPLL). Studied by several authors [1–5], this method is a combination of a PLL and an ILO. The voltage-controlled oscillator (VCO) of such a loop is an injected oscillator [6–9], in contrast to the free-running oscillator of conventional PLLs. A microwave oscillator can be synchronized to an external low-power stable signal, thus providing a low-phase-noise high-power output.

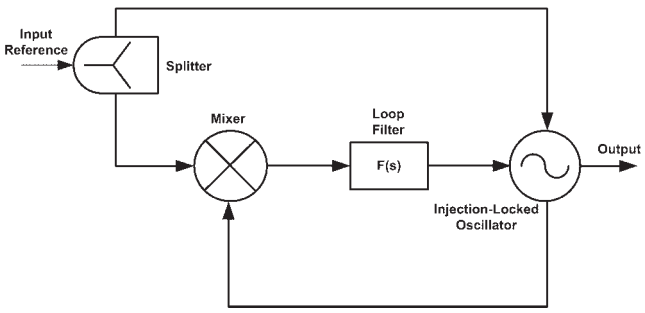

Figure 1 Injection-locked synthesizer

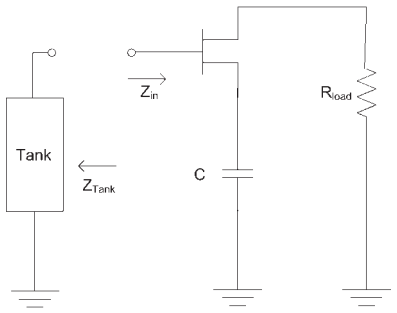

Figure 2 Common-source capacitive feedback oscillator

The input reference signal is divided into two parts using a power splitter. One part is used to provide the reference signal to the mixer, which acts like a phase detector, whereas the other part is injected into the VCO. The mixer produces a phase-error signal that is processed by the loop filter and tunes the VCO.

Huang [1] reported the nonlinear analysis of a MESFET injection locked oscillator at 2.7 GHz, whereas Razavi [2] presented the injection-pulling phenomena of a 1-GHz phase-locked oscillator. Optically injected and phase-locked combined systems have been extensively reviewed by Blanchflower [2] and Ramos [3]. Finally, a 10-GHz injection-locked phase-locked oscillator was analyzed and demonstrated in [5], where the same device is used as both phase detector and oscillator.

In this paper, we develop a different approach for ILPLL design at 5 GHz by applying a technique used in optical communications [3, 4]. The proposed system, as shown in Figure 1, is suitable for synthesizer applications at 5 GHz due to its implementation characteristics. Furthermore, we newly address the phase-noise analysis of ILPLLs using the loop linear model and compare the results with previously reported work. The analytical expression for the locking range is also derived and the pulling behavior of the injected oscillator is demonstrated.

For the experimental investigation, a prototype was implemented using commercial components. The measurement results illustrate the capability of the proposed analysis to accurately predict the phase-noise performance, demonstrate the main characteristics, and confirm the feasibility of the system.

The contents of this paper are as follows. In section 2, we present the design and synchronization of the oscillator, which is one of the most critical parts of the proposed circuit. The phase-noise model and locking-range analysis are then proposed in section 3. Section 4 reports the implementation and experimental results, while the conclusions are presented in section 5.

2. DESIGN AND SYNCHRONIZATION OF THE OSCILLATOR

2.1. The Oscillator

A common-source capacitive feedback oscillator, illustrated in Figure 2, is employed by using a GaAs Hetero-Junction FET with a parallel resonant applied at the gate.

The equivalent circuit of the tank, which consists of a hyperabrupt GaAs tuning varactor (with γ equal to 1.25) and an inductor, is shown in Figure 3. $C_s(V)$ is the variable capacitor, C_p and L_s are the parasitic capacitor and inductor, respectively, and $R_s(V)$ is the voltage-dependent resistor. Finally, L is the external inductor. The tuning voltage V can vary from 0 to 7 V.

Initially, the unstable condition

$$R_{\tan k} + R_{in} < 0 \tag{1}$$